On the detectability of the Earth's core signal using space gravity measurements

H Lecomte, S Rosat, M Mandea

2021 AGU Fall Meeting - 15 December 2021 - New Orleans - Poster #DI35D-0054

On the detectability of the Earth's core signal using space gravity measurements

H. Lecomte(1), S. Rosat(1), M. Mandea(2)

(1) University of Strasbourg, ITES (CNRS UMR7063), Strasbourg, France (hlecomte@unistra.fr, severine.rosat@unistra.fr)

(2) CNES, French Space Agency (mioara.mandea@cnes.fr)

Institut Terre & Environnement de Strasbourg | ITES | UMR 7063 de l'Université de Strasbourg & CNRS & ENGEES

Introduction

In 2012, a study by Mandea et al. highlighted a possible correlation between the variations of the magnetic and the gravity fields. It showed a large pattern of similarities on the South of Africa at interannual time and large spatial scales. Such correlations might be induced by processes that create geomagnetic jerks or, for example, dissolution-crystallization processes at the core-mantle boundary. [2]

Since then, satellites have continued to record and we acquired 10 more years of data to analyze. We also benefit from an improvement in the modeling of magnetic and gravity fields variations. With all these additions, we reproduce this past study to update our knowledge of these correlations.

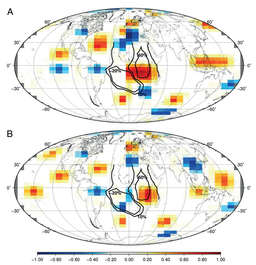

Fig. 1. Correlation between the GRACE gravity anomaly series and the secular acceleration of the vertical downward geomagnetic field component. All correlation values that are not significant at the 95% level have been set to zero.
[1]

Data

$$V(\lambda,\theta,r) = \sum_{l=0}^{+\infty} A_l \sum_{m=0}^{+\infty} [C_{l,m}cos(m\lambda) + S_{l,m}sin(m\lambda)]P_{l,m}(cos\ \theta)$$

$$B(\lambda,\theta,r) = \sum_{n=1}^{+\infty} A_l \sum_{m=0}^{+\infty} [g_{l,m}cos(m\lambda) + h_{l,m}sin(m\lambda)]P_{n,m}(cos\ \theta)$$

COST-G monthly (2002 – 2019)		[3]
Spherical harmonics representation, l_{max} = 60		Ref
$C_{2,0}$	TN14 GSFC	[4]
$C_{3,0}$ acc. failure	TN14 GSFC	[4]
$C_{2,1}/S_{2,1}$ acc. failure	UT/CSR SLR product	[5]
Oceanic loading	AOD1B GAB (MPIOM)	[6]
Atmospheric loading	AOD1B GAA (ERA-Interim)	[6]
Hydrology	ISBA-CTRIP	[7]
GIA	remove trends	

Variations of the gravity field have been measured by GRACE and GRACE Follow-On missions and are caused by several processes listed in Fig. 3. To access the variations caused by internal sources, we must minimize the external signals. Since we are interested in **interannual and large spatial scales**, this reduces the number of signals to consider : atmosphere, oceanic and hydrological loading and post-glacial rebound (GIA trend).

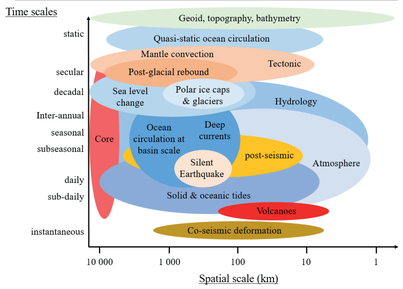

Fig. 3. Spatial and temporal scales of the physical processes causing mass variations in the Earth system

Variations of the magnetic field have been measured by several satellites since 2002. They are used to build models of the core magnetic field. We use the CHAOS-7.8 model [8] to retrieve the secular acceleration $\partial^2_t B$ up to n = 8 with Gauss coefficients. Magnetic variations from the oceans and the lithosphere are negligible (< 5% of the total signal).

Filtering of gravity data

Variations of the magnetic field do not need to be filtered as they already only include large spatial scales and interannual signals.

However, we need to filter the gravity field variations as the dominant signal is mainly annual variations. We use a Gaussian kernel of radius 1200 km applied by convolution to the products which removes spherical degrees larger than 13.

Temporal variations of the gravity field are low-pass filtered with a Butterworth filter whose cut-off frequency is 0.5 cycle per year.

Time series

We have reconstructed the gravity and magnetic time series on a global grid defined at 10° in latitude and 20° in longitude (Fig. 4). Higher latitudes are not shown because the signal/noise ratio is lower.

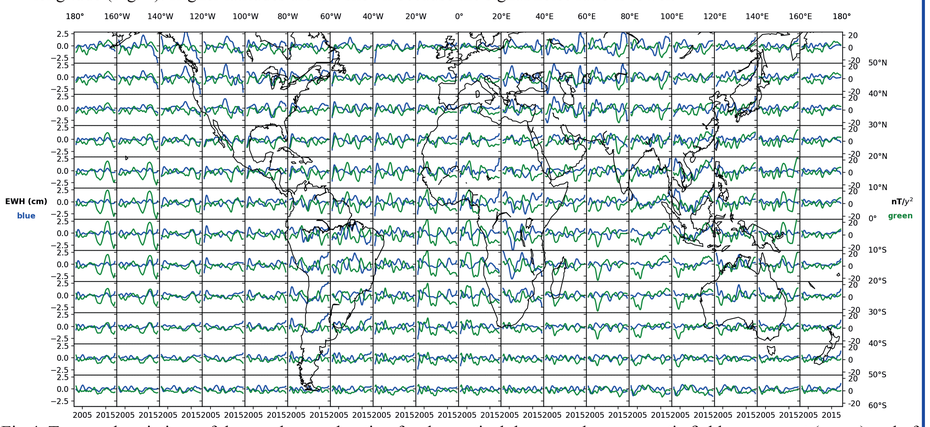

Fig.4. Temporal variations of the secular acceleration for the vertical downward geomagnetic field component (green) and of the COST-G gravity anomalies (blue), at center of cell position. Each series starts in August 2002 and ends in August 2018.

Fig. 5 shows maps of the root mean square (RMS) values of each products. For the magnetic field, large variations are located near the equator (Fig. 5a). For the gravity field, the largest signals are located on the continents (Fig. 5b). It is most likely hydrological interannual variations non-modelized by ISBA model.

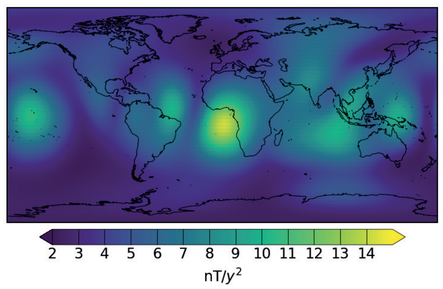

Fig. 5a. RMS map of CHAOS-7.8 secular acceleration

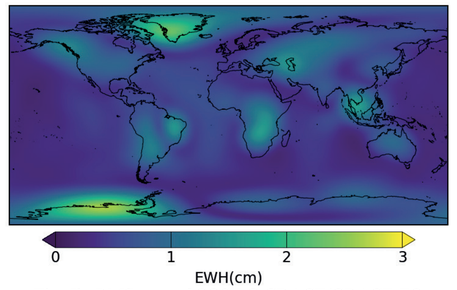

Fig. 5b. RMS map of COST-G GRACE/GRACE-FO products

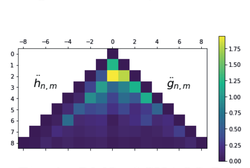

Fig. 6a. RMS of CHAOS-7.8 coefficients of the secular acceleration

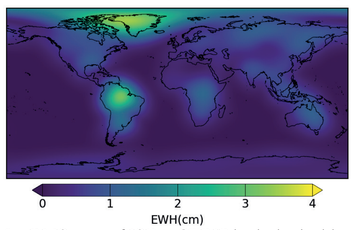

Fig. 5c. RMS map of ISBA-CTRIP hydrological loading

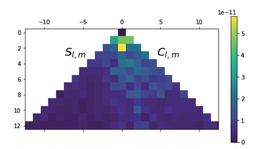

Fig. 6b. RMS of COST-G coefficients

Spherical harmonics correlation

We observe the largest correlation (0.65) between coefficients $C_{6,2}$ and $g_{6,2}$. Gravity $C_{6,2}$ coefficient also contains a periodic oscillation close to 3 years, not present in the magnetic field $g_{6,2}$ coefficient. Note also that both coefficients do not have a large amplitude compared to others.

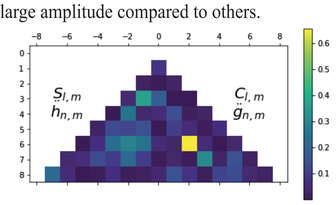

Fig. 7 .Correlation between coefficients of COST-G and CHAOS7.8

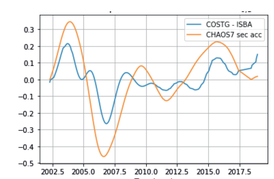

Fig. 8. $C_{6,2}$ and $g_{6,2}$ with adjusted scale

Spatial correlation

Fig. 9 shows the correlation map between magnetic and gravity time-series. Latitudes higher than 60° are not shown because the signal/noise ratio is lower. Fig. 9a shows correlation between COST-G product minus ISBA hydrological loading and magnetic secular acceleration. Fig. 9b shows correlation between ISBA hydrological loading and magnetic field secular acceleration.

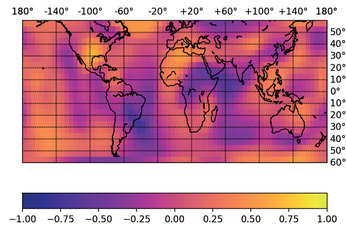

Fig. 9a. Correlation map between GRACE minus ISBA gravity anomalies and secular magnetic acceleration

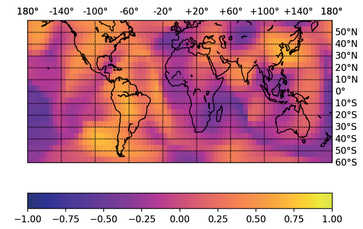

Fig. 9b. Correlation map between ISBA hydrological loading and magnetic secular acceleration

Fig. 9a shows two areas of anti-correlation in the East of Africa and in the South of Brazil. These two areas are associated with low signals for both gravity and magnetic variations. A small area of positive correlation can also be found in the West of New Orleans.

Fig. 9b shows two larges areas of correlation in Amazonie and in East-Asia between hydrological loading and magnetic secular acceleration. The magnetic acceleration amplitude is not very large in those areas.

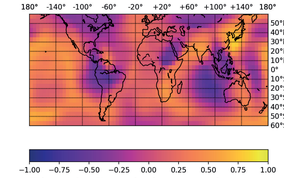

Fig. 10. Correlation map between GAB oceanic loading and secular magnetic acceleration

Fig. 10 shows shows correlation between AOD1B GAB oceanic loading and magnetic field secular acceleration.

It show one area of anti-correlation in India Ocean and an area of correlation in center Pacific Ocean.

Conclusions

At this stage of the study, with new data sets and methods, we are not able to recover the same results as [1]. Further tests need to be performed to investigate the difference between the two studies. Mainly, the differences reside in the temporal filtering and the hydrological loading model used (here ISBA-CTRIP while GLDAS2 was used in [1]).

A correlation has been found between $C_{6,2}$ and $g_{6,2}$ but these coefficients do not have a large amplitude. It could simply be a residual noise correlation. Theoretical analysis such as [9] predicts contributions from the core processes on degree 2 are below the accuracy of products.

Spatial correlation has also been found over low-signals areas which mainly indicates a spurious correlation due to some unmodeled gravity hydrological residuals.

Further investigation will be conducted on the following points:

- Core dynamics or CMB processes that can generate global mass redistribution [9].
- Possible correlation between the magnetic field and the oceanic loading from models.

Highlighting new correlations between geomagnetic and geodetic signals can point the direction.

Bibliography

[1]M. Mandea, I. Panet, V. Lesur, O. de Viron, M. Diament, and J.-L. L. Mouël, "Recent changes of the Earth's core derived from satellite observations of magnetic and gravity fields," Proceedings of the National Academy of Sciences, vol. 109, no. 47, pp. 19129–19133, Nov. 2012, doi: 10.1073/pnas.1207346109.
[2]M. Mandea, C. Narteau, I. Panet, and J.-L. Le Mouël, "Gravimetric and magnetic anomalies produced by dissolution-crystallization at the core-mantle boundary," Journal of Geophysical Research: Solid Earth, vol. 120, no. 9, pp. 5983–6000, 2015, doi: https://doi.org/10.1002/2015JB012048.
[3]U. Meyer et al., International Combination Service for Time-variable Gravity Fields (COST-G) Monthly GRACE Series. 2020. doi: 10.5880/ICGEM.COST-G.001.
[4]B. D. Loomis, K. E. Rachlin, D. N. Wiese, F. W. Landerer, and S. B. Luthcke, "Replacing GRACE/GRACE-FO With Satellite Laser Ranging: Impacts on Antarctic Ice Sheet Mass Change," Geophysical Research Letters, vol. 47, no. 3, p. e2019GL085488, 2020, doi: 10.1029/2019GL085488.
[5]B. D. Loomis, K. E. Rachlin, and S. B. Luthcke, "Improved Earth Oblateness Rate Reveals Increased Ice Sheet Losses and Mass-Driven Sea Level Rise," Geophysical Research Letters, vol. 46, no. 12, pp. 6910–6917, 2019, doi: https://doi.org/10.1029/2019GL082929.
[6]H. Dobslaw et al., "A new high-resolution model of non-tidal atmosphere and ocean mass variability for de-aliasing of satellite gravity observations: AOD1B RL06," Geophysical Journal International, vol. 211, no. 1, pp. 263–269, Oct. 2017, doi: 10.1093/gji/ggx302.
[7]B. Decharme et al., "Recent Changes in the ISBA-CTRIP Land Surface System for Use in the CNRM-CM6 Climate Model and in Global Off-Line Hydrological Applications," Journal of Advances in Modeling Earth Systems, vol. 11, no. 5, pp. 1207–1252, 2019, doi: 10.1029/2018MS001545.
[8]C. C. Finlay et al., "The CHAOS-7 geomagnetic field model and observed changes in the South Atlantic Anomaly," Earth, Planets and Space, vol. 72, 2020.
[9]M. Dumberry and M. Mandea, "Gravity Variations and Ground Deformations Resulting from Core Dynamics," Surveys in Geophysics, pp. 1–35, 2021.